Hybrid optical and acoustic resolution optoacoustic endoscopy

HAILONG HE,[1,2] GEORG WISSMEYER,[1,2] SAAK V. OVSEPIAN,[1,2] ANDREAS BUEHLER,[1,2] VASILIS NTZIACHRISTOS[1,2,*]

[1] *Institute for Biological and Medical Imaging, Helmholtz Zentrum München, Ingoldstädter Landstraße 1, 85764 Neuherberg, Germany*

[2] *Chair for Biological Imaging, Technische Universität München, Ismaninger Str. 22, 81675 München, Germany*
**Corresponding author: v.ntziachristos@tum.de*

We propose the implementation of hybrid optical and acoustic resolution optoacoustic endoscopy. Laser light is transmitted to tissue by two types of illumination for achieving optical and acoustic resolution imaging. A 20 MHz ultrasound detector is used for recording optoacoustic signals. The endoscopy probe attains 3.6 mm diameter and is fully encapsulated into a catheter system. We validate the imaging performance of the hybrid endoscope on phantoms and ex vivo and discuss the necessity for the extended resolution and depth range of endoscopy achieved.

OCIS codes: *(170.5120) Photoacoustic imaging; (170.2150) Endoscopic imaging; (110.4190) Multiple imaging.*

http://dx.doi.org/10.1364/OL.99.099999

High-resolution optical imaging techniques (e.g., white-light endoscopy, fluorescence microscopy, multi-photon microscopy or confocal microscopy) are commonly employed for endoscopic applications [1, 2]. White light endoscopy (WLE) allows the collection of color video of the entire gastro-intestinal track and can inspect for obstructions and overt stress and damage of the tissue, however it is only capable of visualizing the lumen surface. Confocal laser endomicroscopy (CLE) could visualize subsurface lumen morphology leading to earlier detection of latent gastrointestinal pathologies or prodromal cancers [2]. However, due to intrinsic limitations of photon propagation in tissues, CLE has limited imaging penetration depth and only interrogates small superficial lumen volumes (<0.1mm^3) at a time, which prevents application to surveillance endoscopy. The use of fluorescence imaging has a promising outlook for endoscopic surveillance, especially when utilizing systemic or local administration of agents with disease specificity [2]. Nevertheless, fluorescence imaging is two-dimensional in nature and the administration of fluorescence agents comes with a higher threshold of regulatory processes compared to label-free lumen inspection.

Optoacoustic imaging allows high-resolution interrogation much deeper than intra-vital microscopy and can visualize intrinsic contrast, thus operating in label-free mode [3]. Detection of pathophysiological aberrations can be enhanced by spectral imaging. In particular, multispectral optoacoustic tomography (MSOT) can identify hemoglobin and potentially other tissue chromophores, revealing tissue hypoxia, ischemia or perfusion in-vivo [3, 4]. Engineered contrast using reporter-gene methods or externally administered agents has also been reported [3-5].

Optoacoustic endoscopes operating on ultrasonic diffraction limitations using focused ultrasound detectors, achieve lateral resolution spanning from hundreds to tens of micro-meters with an imaging depth up to several millimeters. Such acoustic resolution optoacoustic endoscopes (AR-OE) have been showcased to provide high resolution visualization of the intestinal vasculature of small animals in vivo [6-9].Even higher resolution can be achieved by optical-resolution optoacoustic endoscopy (OR-OE) using a focused laser beam, in analogy to intra-vital optical microscopy [10-13]. However, as intra-vital microscopy, OR-OE is affected by light scattering in tissue and thus limited to superficial structures. Herein, we propose an optical resolution (OR) and acoustic resolution (AR) optoacoustic endoscope appropriate for improving the endoscopic depth and resolution range.

Fig. 1(a) presents the schematic overview of the OR/AR-endoscope. A custom-designed unfocused ultrasound transducer (Imasonic, France) with a center frequency of 20 MHz is used for the detection of ultrasound signals. The diameter of the transducer is 2 mm and the sensing area has a rectangular shape with a length of 0.25 mm and a width of 1.6 mm, yielding an acceptance angle of 80 degrees as derived experimentally from point-source measurements. A GRIN-lens fiber (GT-MMFP-10 μm, GRINTECH, Germany) is secured beneath the transducer for OR illumination. This fiber has a core diameter of 10 μm, a numerical aperture of 0.1, and consisting of a gradient index lens, a coreless spacer and a prism. To align the illumination focus, the GRIN-lens is placed with a tilt angle of 5 degrees in relation to the transducer. Such arrangement prevents the fiber tip from blocking the transmission path of optoacoustic signals. Using a beam profiler (SP620U, OPHIR Beam Gauge, US), we measured the beam diameter based on the full width at half-maximum (FWHM) value, which at the focus region estimates to be ~8.7 μm (Fig. 1(b)). For implementing AR imaging, a multi-mode fiber (400 μm diameter) with a broad

side-view illumination has been aligned with the transducer at a tilt angle of 30 degrees. With such an arrangement, the overlapping areas between the laser beam and the acoustic axis begin at about 1 mm distance from the transducer sensing surface, and extend over a large depth. Illumination is provided by a 532 nm laser, with a pulse repetition rate of 2 kHz and energy of 1 mJ/pulse and pulse width of 0.9 ns (Wedge HB532, BrightSolutions SRL, Pavia, Italy). The beam is attenuated, collimated and guided through a pinhole (Thorlabs) to ensure spatial filtering. It is then passed into a telescopic lens array (Thorlabs) to adjust the beam diameter to match the back aperture of a low NA microscope objective (L-4X, Newport) which is mounted on a manual fiber coupler (F-91TS, Newport). Finally, the beam is tightly focused and coupled into the OR and AR fibers respectively. The light fluence at the surface of the sample is measured about 10 mJ/cm2 for OR imaging and about 6 mJ/cm2 for AR imaging. The recorded optoacoustic signals without averaging are amplified by a low noise amplifier (63 dB, AU-1291, Miteq Inc., Hauppauge, New York, USA) and sampled by a high-speed digitizer, operating at 1 GS/s (NI PCI-5124, USA; 12 bit resolution; max sampling rate 4 GS/s).

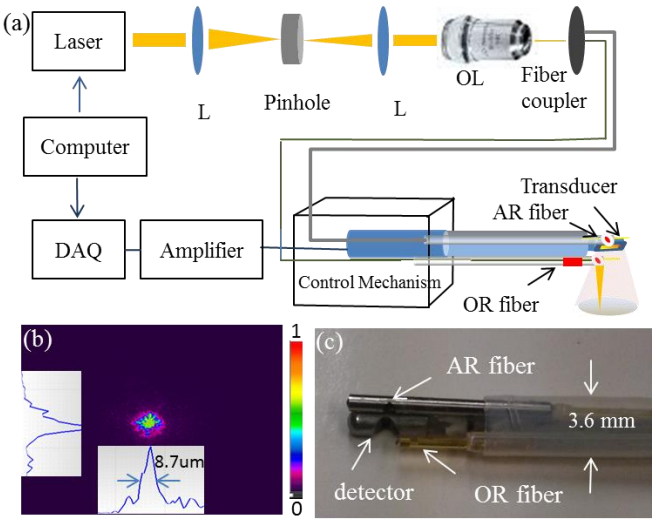

Fig. 1. (a) Schematic illustration of the imaging setup with alignment of various modules; Abbreviations: L, Lens; OL, objective lens. (b) Laser beam intensity profile at the focal distance. (c) Photograph of the distal end of the hybrid endoscopy probe.

The endoscope probe is encapsulated in a medical-grade (polyethylene terephthalate) tube with an outer diameter of 3.6 mm, which can readily pass through 3.8 mm working channels of commercial video endoscopes. Fig.1(c) shows the enlarged photograph of the probe. To obtain volumetric images, fast linear and rotational stages (Oriental Motor, Japan) were employed. The probe is first scanned linearly along the direction of the lumen and then rotated to get adjacent cross-sectional images. This scanning mode is suitable only for limited-view imaging of the lumen volume, i.e. an imaging mode that is appropriate for operation under optical endoscope guidance, whereby the hybrid optoacoustic endoscope is operated through the working channel of an optical endoscope. However, 360 degrees rotation could be also contemplated for endoscopes designed to operate in stand-alone mode, i.e. without white-light endoscopy guidance. In the current implementation, OR and AR scans are performed by sequentially coupling the light into the corresponding fiber. The linear and rotational scanning step sizes are 0.01 mm and 0.01 degrees for OR imaging, and 0.08 mm and 0.1 degrees for the AR imaging. Hilbert transform is performed to process the OR data; the filtered back-projection method is used to reconstruct the AR data as described previously[14].

To characterize the resolution of the system, we measured a phantom with several sutures (10 μm diameter) embedded in scattering agar (6% intra-lipid) at different depths (0.3 mm to 4 mm). The suture positions are illustrated in Fig. 2(a). In order to quantify the OR resolution, point-spread-functions (PSFs) were measured by imaging the first suture at different distances from the OR fiber. Fig. 2(b, c) present the OR images with results of these measurements. As evident, the width of PSF shows a clear depth-dependency following the diameter variation of the laser beam, and the corresponding beam diameter characterized as FWHM along the depth direction is depicted in Fig. 2(c). The highest signal intensity corresponds to the focal distance of the optical illumination (i.e., 0.8 mm from the probe surface), as indicated by the white arrow in Fig. 2(b). From this specific position, the lateral resolution was estimated to be 13 μm, as illustrated in the inset of Fig. 2(c). To determine the combined OR and AR resolution, a B-scan image of the phantom was obtained and shown in Fig. 2(d). The detector was kept at 0.5 mm distance from the phantom surface. OR readouts are presented in green while AR measurements are marked in red. As evident, the OR mode can only resolve the first suture because of optical scattering. The AR mode on the other hand can image much deeper, obtaining a lateral resolution of ~250 μm at depths of at 1.5 mm. Fig. 2(e) presents the AR resolution as a function of the imaging depth. To demonstrate the volumetric imaging ability of the hybrid endoscope, a four suture phantom was imaged as illustrated in the Fig. 2(f, inset). The phantom was built by fixing sutures (10 μm in diameter) at two different layers of ~1 mm separation. Afterwards, the sutures were arranged in a luminal structure, and were scanned cylindrically over 10 degrees. Fig. 2(f) depicts the corresponding 3D image, showing the overlay of the OR and AR optoacoustic scans.

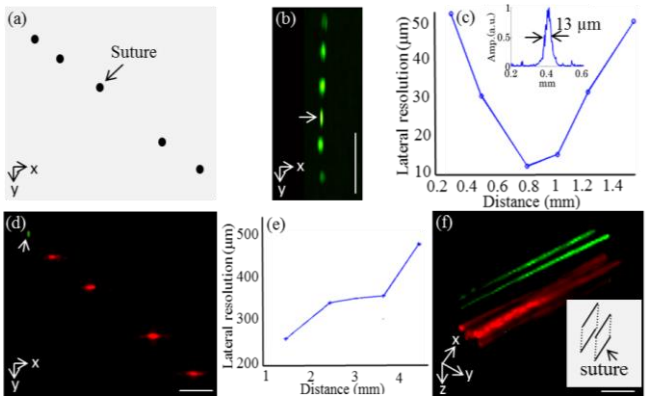

Fig. 2. (a) A schematic illustration of the suture phantom. (b) Optoacoustic images of a 10 μm suture imaged with OR illumination at different depths, scale bar 500 μm. (c) Graphical representation of the OR beam diameter characterized as FWHM along with the depth direction. The inset shows a lateral line profile of the suture (indicated

by the white arrow in (b)) in the focus region of the GRIN fiber. (d) Optoacoustic images of sutures acquired at different depths with OR and AR illumination, the +y axis corresponds to depth direction, scale bar 1mm. (e) Lateral AR resolution graph along the depth direction. (f) The corresponding 3D image, showing the overlay of normalized OR and AR optoacoustic images of the suture phantom; the +z axis corresponds to depth direction; scale bar 1mm. The OR images are presented in green while the AR image are in red.

In order to assess the imaging performance of the system on biological specimens, a fresh mouse ear ex vivo was imaged. A luminal structure was casted by rolling the mouse ear inside of a plastic tube. A photograph of the ear imaged prior to rolling was shown in Fig. 3(a). Volumetric images were then obtained by scanning the probe cylindrically over 20 degrees and linearly along the lumen longitudinal dimension over 3 mm, with the distance between the mouse ear and the probe kept about 1mm during scanning. By linearly pulling the probe, we acquired sectional images [indicated by the dash line in Fig. 3(b)] in the AR and OR mode respectively, which are displayed in Fig. 3(d) and 3(e). The maximal amplitude projections of the volumetric images acquired in AR and OR modes are shown in Fig. 3(b) and (c) respectively. As can be seen, the AR image resolved the large vessels, which accurately matched those visible in the photograph. Of note, numerous smaller vessels are distinguishable on the OR image, which are not visible on the AR readouts (e.g. indicated by the white arrow in Fig. 3(c)).

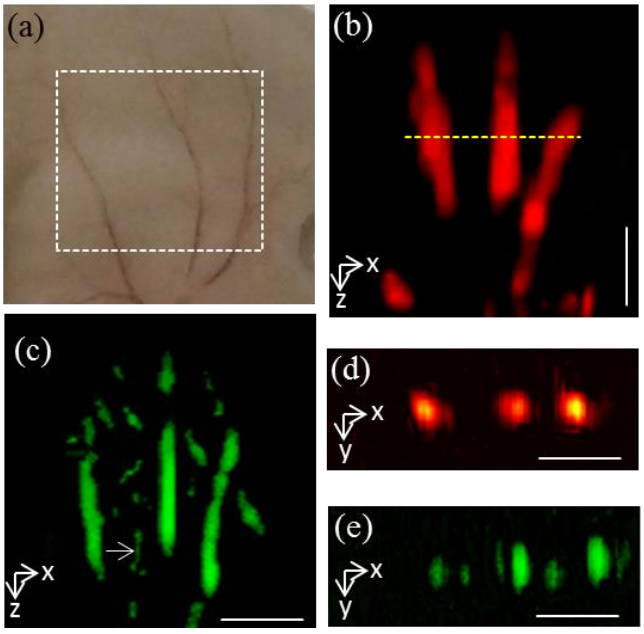

Fig. 3. Optoacoustic images of a mouse ear ex vivo. (a) The photograph of the mouse ear shows the scanning area (highlighted by a dash square). (b) and (c) Volumetric maximal amplitude projection images acquired in AR and OR mode respectively, from the mouse ear boxed by the dash square in (a). (d) and (e) Corresponding AR and OR sectional images in the position marked by the yellow dash line in (b). Red and green colors represent the AR and OR images, respectively. Scale bar 500 μm.

The data presented herein for the first time to our knowledge demonstrate the feasibility of hybrid optical resolution and acoustic resolution optoacoustic endoscopy with a single sensor. The probe has a diameter of 3.6 mm, which is compatible with the working channel of white-light optical endoscopes. As shown, by focusing the laser light with the GRIN fiber, an optical resolution of the order of 13 μm can be achieved, with an impressive SNR of 20 dB (determined based on the ratio of the peak signal intensity and average noise) based on the characterization of a 10 μm diameter suture with the laser energy below the ANSI safety limit (20 mJ/cm2). The results of the phantoms and mouse ear measurements ex vivo show that proposed herein hybrid endoscopy system can gain optical resolution imaging of the surface and tomography imaging for the deeper features. It should be noted that, due to the short working distance of the OR fiber, the probe in the current implementation has to be close to the sample surface, thus only a limited luminal segment can be imaged at a time. To improve the applicability of the presented endoscope for obtaining circumferential images of the big lumen, a GRIN fiber with longer focal distance should be applied. Besides, advanced ultrasound transducers, such as optical interferometry based ultrasound detectors, could increase both the sensitivity and AR resolution[15]. Furthermore, beam-splitting or preferably two time-interleaved laser sources could be employed for concurrent imaging, which can further improve imaging efficiency. Presented herein concept of using two different fibers to achieve dual OR and AR imaging can improve endoscopic applications, yielding additional information inaccessible to previous implementations.

Funding. The research leading to these results has received funding from the European Union project FAMOS (FP7 ICT, contract no. 317744).

References

1. P. Amornphimoltham, A. Masedunskas, and R. Weigert, Advanced drug delivery reviews 63, 119-128 (2011).
2. A. Hoffman, M. Goetz, M. Vieth, P. R. Galle, M. F. Neurath, and R. Kiesslich, Endoscopy 38, 1275-1283 (2006).
3. A. Taruttis and V. Ntziachristos, Nature Photonics 9, 219-227 (2015).
4. A. Taruttis, G. M. van Dam, and V. Ntziachristos, Cancer research 75, 1548-1559 (2015).
5. A. Liopo, R. Su, and A. A. Oraevsky, Photoacoustics 3, 35-43 (2015).
6. J. M. Yang, C. Favazza, R. Chen, J. Yao, X. Cai, K. Maslov, Q. Zhou, K. K. Shung, and L. V. Wang, Nature medicine 18, 1297-1302 (2012).
7. H. He, A. Buehler, and V. Ntziachristos, Opt Lett 40, 4667-4670 (2015).
8. J. M. Yang, C. Li, R. Chen, Q. Zhou, K. K. Shung, and L. V. Wang, Journal of biomedical optics 19, 066001 (2014).
9. B. Dong, S. Chen, Z. Zhang, C. Sun, and H. F. Zhang, Opt Lett 39, 4372-4375 (2014).
10. D. Soliman, G. J. Tserevelakis, M. Omar, and V. Ntziachristos, Scientific reports 5, 12902 (2015).
11. E. M. Strohm, M. J. Moore, and M. C. Kolios, Photoacoustics (2016).
12. P. Hajireza, W. Shi, and R. Zemp, Laser Physics Letters 10, 055603 (2013).
13. J. M. Yang, C. Li, R. Chen, B. Rao, J. Yao, C. H. Yeh, A. Danielli, K. Maslov, Q. Zhou, K. K. Shung, and L. V. Wang, Biomedical optics express 6, 918-932 (2015).
14. M. Xu and L. Wang, Physical Review E 71(2005).
15. A. Rosenthal, S. Kellnberger, D. Bozhko, A. Chekkoury, M. Omar, D. Razansky, and V. Ntziachristos, Laser & Photonics Reviews 8, 450-457 (2014).